

Articles

A Comparative Study of Copper-Promoted Water–Gas-Shift (WGS) Catalysts

Prashant Kumar*[‡] and Raphael Idem[†]

Hydrogen Production Research Group, Process Systems Engineering Laboratory, Faculty of Engineering, University of Regina, Regina, SK, Canada S4S 0A2, and HTC Purenergy, #001, 2305 Victoria Avenue, Regina, SK, Canada S4P 0S7

Received August 16, 2006. Revised Manuscript Received January 8, 2007

We studied the catalytic water–gas shift reaction over commercial Cu–ZnO–Al₂O₃ (LTS-C) and Cu-promoted Fe–Cr oxide (HTS-C) catalysts as well as a high-temperature Cu-promoted (UFR-C) catalyst developed in our laboratory. The catalysts were characterized by different techniques such as X-ray diffraction, thermogravimetry/differential scanning calorimetry, temperature-programmed reduction, and sorption analyses. The activities of these catalysts were evaluated in the compositions of mole fractions having 2.6–16.8% CO, 45% H₂O, and the balance nitrogen in the range of 473–973 K. It was observed that the reduction temperature, the ratio of the mass of the catalyst to the mass flow rate of CO ($g_{\text{cat}}/h/\text{mol of CO}$), and CO concentrations have significant effects on the catalytic activities. In the presence of 2.6% CO, the Cu–ZnO–Al₂O₃ catalyst was most active at 473 K while the Cu-promoted Fe–Cr oxide catalyst was most active at 773 K. The catalytic activities of HTS-C and LTS-C were compared with that of UFR-C in the presence of both CO in different concentrations and reformat streams as a feed. The results showed that ceria–zirconia-supported non-noble metal catalysts can give very high water–gas shift activity at very short contact times compared to that of the commercial water–gas shift catalyst.

1. Introduction

One of the many possible reasons leading to the catastrophic destruction caused by the recent hurricanes Katrina and Rita could be global warming and its overall impact on climate change. However, in the past few decades or so, considerable attention has been paid to the reduction of pollutants emissions originating either from stationary power plants that are based on the combustion of fossil fuels or from mobile sources such as in the use of internal combustion engines for combusting fossil fuels.^{1–2} The use of hydrogen as a fuel for the future has generated a lot of promise, especially if it is used for fuel-cell applications.^{3–5} A fuel cell is an efficient energy conversion device. Among the many fuel cells available, the proton exchange membrane (PEM) fuel cell is reported to have an overall energy efficiency of 60% when used with ultrapure hydrogen as the fuel.⁶ Moreover, PEM fuel cells are also attractive for use in transport applications. Since water is the only emission, it means hydrogen has a significant future

potential as an alternative fuel that can probably solve the problems of CO₂ emissions as well as the other air contaminants.

Hydrogen (H₂) is primarily produced through steam reforming of natural gas (mainly CH₄).⁷ Dry reforming of natural gas (in the presence of CO₂) is another approach for producing H₂.⁸ Similarly, on-board or off-board steam reforming of methanol, gasoline, and diesel is an option, especially for automobiles which are likely to use PEM fuel cells.^{9,10} However, the H₂ produced from these reformation processes contains typically about 5–20% carbon monoxide (CO) by volume, and therefore, additional processing of the reformat is required to reduce the CO concentration to ~10 ppmv so that the performance loss due to CO poisoning of the PEM fuel cell anode catalyst can be minimized. A recent study⁶ has confirmed a performance loss of PEM fuel cells of 20% within 200 h when the CO concentration is more than 10 ppmv. The water–gas shift (WGS) reaction ($\text{CO} + \text{H}_2\text{O} \leftrightarrow \text{CO}_2 + \text{H}_2$) is generally used in many fuel-processing schemes to reduce the concentration of CO to 0.5–1% (5000–10000 ppmv). The reaction is moderately exothermic ($\Delta H = -41.1$ kJ/mol) and equilibrium-limited, and therefore, low CO levels can only be achieved at low temperatures, even though the kinetics are more favorable at higher temperatures. As a result, two WGS reactors are typically used

* Corresponding author phone: 1-306-337-2594; fax: 1-306-337-3112; e-mail: prashant.kumar@uregina.ca.

[†] University of Regina.

[‡] HTC Purenergy.

(1) Song, C. *Catal. Today* **2002**, *77*, 17.

(2) Breen, J. P.; Ross, J. R. H. *Catal. Today* **1999**, *51*, 521.

(3) de Wild, P. J.; Verhaak, M. J. F. M. *Catal. Today* **2000**, *60*, 3.

(4) Agrell, J.; Birgersson, H.; Boutonnet, M.; Melian-Cabrera, I.; Navarro, R. M.; Fierro, J. L. G. *J. Catal.* **2003**, *219*, 389.

(5) Choi, Y.; Stenger, H. G. *Appl. Catal., B* **2002**, *38*, 259.

(6) Pasel, J.; Cremer, P.; Wegner, B.; Peters, R.; Stolen, D. *J. Power Sources* **2004**, *126*, 112.

(7) Sehested, J. *Catal. Today* **2006**, *111*, 103.

(8) Hu, Y. H.; Ruckenstein, E. *Adv. Catal.* **2004**, *48*, 297.

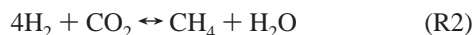
(9) Adesina, P. A. A.; Trimm, D. L.; Cant, N. W. *Chem. Eng. J.* **2004**, *99*, 131.

(10) Puranama, H.; Ressler, T.; Jenoft, R. E.; Soerijanto, H.; Schlogl, R.; Schomacker, R. *Appl. Catal., A* **2004**, *259*, 83.

in industry: a high-temperature shift (HTS) reactor, operating at 340–530 °C, for rapid CO conversion, and a low-temperature shift (LTS) reactor, operating at 180–230 °C, in order to achieve lower equilibrium CO contents.¹¹ Conventional HTS catalysts, usually Cu-promoted Fe–Cr oxide (HTS-C), are inactive at temperatures below 300 °C, while Cu–ZnO–Al₂O₃ catalysts (LTS-C) used for LTS degrade above 250 °C.¹² A further reduction in CO concentration following WGS is made possible either by catalytic selective routes such as preferential oxidizers (CO + 1/2O₂ → CO₂), also called PROX, or physical routes like membrane separation.^{13–14} However, the main disadvantage of using PROX is hydrogen combustion (H₂ + 1/2O₂ → H₂O), an undesirable reaction. Another problem associated with PROX is the reversed WGS, which becomes very large as the CO concentration approaches zero.¹⁵ On the other hand, for high-temperature WGS, reduced equilibrium is overcome by product H₂ removal via the membrane, making it more attractive, especially from the purity point of view.¹⁶ Another problem generally associated with high-temperature WGS is methanation, which can reduce the hydrogen yield and can also increase the temperature of the catalyst, thereby lowering the efficiency of hydrogen production.



Both the commercial HTS-C and LTS-C have certain drawbacks



that make them unsuitable for fuel processors being developed for use on-board vehicles or for distributed power or hydrogen production.¹⁷ First, these catalysts require an activation step consisting of a controlled in situ reduction. In the reduced state, these catalysts may be pyrophoric or at least exhibit a large rise in temperature when exposed to air.¹⁸ This temperature rise can cause the catalysts to sinter, resulting in loss in activity.¹⁹ Also, during shutdown, these catalysts may be exposed to condensing steam, which can cause the catalyst to reoxidize. Because of frequent startups and shutdowns, these catalysts may be exposed to many condensation and vaporization cycles that can lead to poor mechanical stability.²⁰ It is therefore essential to develop a novel WGS catalyst in order to meet the necessary criteria for use in modern fuel processors. Moreover, we need new catalyst technologies to reform natural gas to fuel-cell-quality hydrogen that will take advantage of our existing fuel infrastructures to ensure a safe and reliable supply to the consumer.

The research in our laboratory^{21,22} for the past few years has focused on this area of high-purity H₂ production for fuel-cell

(11) Newsome, D. S. *Catal. Rev. Sci. Eng.* **1980**, *21*, 275.

(12) Deng, W.; Jesus, J. D.; Saltsburg, H.; Flytzani-Stephanopoulos, M. *Appl. Catal., A* **2005**, *291*, 126.

(13) Huang, J.; El-Azzami, L.; Winton Ho, W. S. *J. Membr. Sci.* **2005**, *261*, 67.

(14) Ma, D.; Lund, C. R. F. *Ind. Eng. Chem. Res.* **2003**, *42*, 711.

(15) Hutelberg, P. C.; Brandin, J. G. M.; Silversand, F. A.; Lundverg, M. *Int. J. Hydrogen Energy* **2005**, *30*, 1235.

(16) Criscuoli, A.; Basile, A.; Drioli, E. *Catal. Today* **2000**, *30*, 53.

(17) Hilaire, S.; Wang, X.; Luo, T.; Gorte, R. J.; Wagner, J. *Appl. Catal., A* **2001**, *215*, 271.

(18) Wang, X.; Gorte, R. J.; Wagner, J. P. *J. Catal.* **2002**, *212*, 225.

(19) Li, Y.; Fu, Q.; Flytzani-Stephanopoulos, M. *Appl. Catal., B* **2000**, *27*, 179.

(20) Fu, Q.; Kudriavtseva, S.; Saltsburg, H.; Flytzani-Stephanopoulos, M. *Chem. Eng. J.* **2003**, *93*, 41.

(21) Aboudheir, A.; Akande, A.; Idem, R.; Dalai, A. *Int. J. Hydrogen Energy* **2006**, *31* (6), 752.

(22) Ibrahim, H. H.; Idem, R. O. *Chem. Eng. Sci.* **2006**, *61*, 5912.

Table 1. Chemical Composition and Physicochemical Properties of the Fresh Catalysts

catalyst	composition of the catalyst (wt %)	S _{BET} (m ² /g)	PV (cm ³ /g)	pore size (nm)	S _{metal} (m ² /g) ^d	dispersion (%) ^b
LTS-C	CuO/ZnO/Al ₂ O ₃ (51/31/18)	88	0.23	9.9	2.6	1.2
HTS-C	CuO/Fe ₂ O ₃ /Cr ₂ O ₃ (3/88/9)	195	0.20	4.0	10.7	3.5
UFR-C	CuO/NiO/ZrO ₂ -CeO ₂ (4.5/2.5/46.5/46.5)	168	0.28	4.2	17.5	7.6

^a Metal surface area determined by H₂ chemisorption with a stoichiometry factor of 2. ^b Ratio between the amount of surface metal and total metal content.

applications from gasoline, diesel, crude ethanol, and natural gas using a dry reformer and hydrogen-permeable membrane coupled with WGS processes when used with novel and advanced modified WGS catalysts. We have recently developed an advanced catalyst system (UFR-C) for use in WGS reactions in the presence of CO₂, H₂, and/or CH₄ together with CO and H₂O in the feed (i.e., reformat gas streams).²³ UFR-C was prepared as meso-structured ceria–zirconia composites assisted by a surfactant.²⁴ Such materials possess good homogeneity and stability, especially after thermal treatment.^{25,26} The intent of this paper is to examine the WGS reaction on the commercial copper-promoted HTS-C and LTS-C catalysts on the reformat gas streams as well as with CO as a feed under similar reaction conditions that we developed for our UFR-C catalysts. This involves measuring the WGS activities of the two commercial catalysts: one Cu–ZnO–Al₂O₃ catalyst used for LTS and another Cu-promoted Fe–Cr oxide catalyst for HTS, respectively, for the CO oxidation in the presence of water in a simulated reformat gas stream. We have also studied how the reduction and reaction temperatures as well as the ratio of the mass of the catalyst to the mass flow rate of CO (W/F_{AO}; g_(cat)/h/mol of CO) affect the CO conversion in general. A comparison of the results with the catalyst developed in our laboratory is also used to validate our claims that the WGS reaction can differ significantly between industrial and fuel-cell related applications. The various parameters and their impact on overall activities of the catalysts are evaluated and discussed in this paper.

2. Experimental

2.1. Catalyst Preparations and Characterizations. Following the work of Terrible et al.,²⁴ we prepared a CeO₂/ZrO₂ mixed oxide of a composition having 50 atom % each. Appropriate amounts of Ce(NO₃)₃·6H₂O and ZrOCl₂·XH₂O dissolved in 500 mL of deionized water each were mixed together to form a clear solution. Similarly, an appropriate amount of cetyltrimethyl ammonium bromide (CTAB) dissolved in 1000 mL of deionized water was then slowly added together (molar ratio of Ce + Zr/CTAB = 0.8) and stirred at room temperature for 90 min. An aqueous solution of ammonia (1200 mL) was then slowly added to the above solution over a period of 120 min. The initial pH before adding the ammonia solution was 2.0 (temperature 34 °C), which increased to 11.6 after the completion of adding the ammonia solution. This caused the precipitation of hydrous cerium–zirconium oxide as a gelatinous yellow-brown solid. After precipitation, the slurry was stirred for 1 h and then sealed in a glass vessel and placed in an oven maintained at 363 K for 5 days in a static position. The mixture was then cooled to room temperature and the precipitate filtered

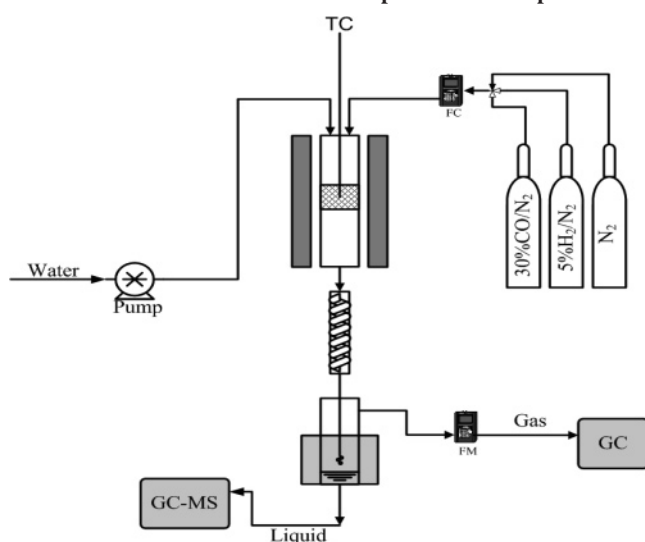
(23) Idem, R.; Kumar, P.; Sun, Y. U.S. Patent Application 20060216227, September 28, 2006.

(24) Terrible, D.; Trovarelli, A.; Llorca, J.; de Leitenburg, C.; Dolcetti, G. *Catal. Today* **1998**, *43*, 1176.

(25) Laosiripojana, N.; Assbunrungrat, S. *Appl. Catal. B*, **2005**, *60*, 107.

(26) Trovarelli, A. *Catal. Rev.-Sci. Eng.* **1996**, *38*, 439.

Scheme 1. Schematic of Experimental Setup



and washed, first with a copious amount of water and then acetone to remove the free surfactant not incorporated within the oxide. The resulting light-yellow powder was dried at 90 °C overnight and calcined in the furnace at 450 °C/4 h under an air flow to remove the surfactant. Nickel (3 wt %) and copper (5 wt %) were then added by using wetness impregnation. The catalyst thus obtained was further calcined at 650 °C for 3 h before use in the reactor. The other two catalysts used for both LTS and HTS were kindly provided by Johnson Matthey Catalysts, IL. All of the catalysts were further characterized using different analytical techniques. Micromeritics ASAP 2010 was used for Brunauer–Emmett–Teller (BET) surface area and chemisorption (using H₂) measurements, whereas thermogravimetric analysis/differential scanning calorimetry (TGA/DSC; TG-DSC-1100, Setaram), temperature-programmed reduction (TPR; Chembet 3000, Quantachrome), and X-ray diffraction (XRD; Bruker, AXS) were used to evaluate other characterizations of the catalysts received. The literature indicates that, apart from N₂O decomposition, there are other methods such as low-temperature oxygen chemisorption and hydrogen chemisorption²⁷ for the determination of metal surface area in supported copper catalysts. Also, the interference of N₂O decomposition in the presence of support having high-surface-area ceria is well-documented in the literature.²⁸ Since the catalyst also contains a low concentration of nickel, hydrogen chemisorption was used in this study to determine the total metal surface area. For hydrogen chemisorption, 0.32 g of fresh catalyst samples (UFR-C) was used at 308 K. Before the isotherms were recorded, samples were evacuated for temperatures up to 573 K under oxygen followed by reduction in flowing H₂ at 923 K. The characterization results obtained are presented in Table 1.

2.2. Experimental Setup. The reaction was carried out using a conventional catalytic fixed-bed tubular reactor operated isothermally at atmospheric pressure (Scheme 1). It was made of an Inconel 625 metal alloy tube of 12.7 mm internal diameter (D) placed vertically in an electric furnace. Reformate as well as CO in nitrogen gas (Praxair) was regulated using a mass flow controller (Aalborg) at the desired flow rate. Three different types of reaction mixtures were used:¹ 5% CO balanced by N₂,² 30% CO balanced by N₂, and³ a simulated reformate stream of 24% CO, 2% CH₄, 1.5% CO₂, and 2.5% H₂ balanced by N₂. Water was pumped through a high-performance liquid chromatography pump (Alltech) at the desired flow rate. The reaction temperature was measured through a sliding thermocouple placed inside the catalyst bed. The error in temperature measurement was within ±1 K.

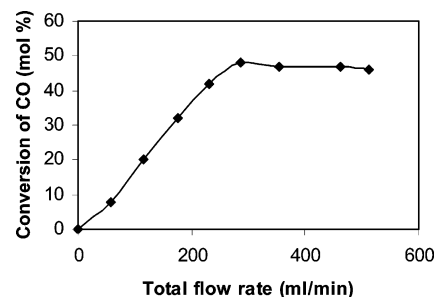


Figure 1. Effect of volumetric feed flow rate on the CO conversion for WGS reaction (30% CO and balance N₂) at 873 K with the constant residence time of 1.3 s.

A typical run for the WGS was performed as follows: approximately 0.25–1.0 g of catalyst (Katalco 83-3M for LTS-C or Katalco 71-5 for HTS-C) of 0.8 mm particle size (D_p) was mixed with approximately 15.0 g of α-Al₂O₃ (as a diluent), kindly provided by Sasol GmbH, Germany, of the same average particle size and loaded into the reactor. This resulted in a catalyst bed height of ~90 mm (L) in the reactor. This also ensured a plug flow behavior in the reactor as the values for L/D_p and D/D_p were more than 50 and 10, respectively. The water and the reaction mixture were fed into the reactor maintained at the reaction temperature at the desired flow rate (161 mL/min for gases and 0.1 mL/min for water). Prior to reaction, the catalyst was activated by in situ reduction with a 5% H₂/N₂ gas mixture (Praxair) flowing at 2.68 × 10⁻⁶ m³/s for 2 h. The reactions were carried out at atmospheric pressure with W/A₀ from 0.88 to 49.96 kg (cat) h/kmol at temperatures in the range of 473–973 K. The product mixture during reaction was passed through a condenser and gas–liquid separator to separate the condensed water and the gaseous product for gas analyses, which was done by on-line gas chromatography (HP 6890) using molecular sieve and Haysep columns coupled with a thermal conductivity detector and helium as the carrier gas. Methane formation was found to be negligible at all temperatures when pure CO as a feed was used under the reaction conditions established. The CO conversion and H₂ selectivity were calculated using the formulas as follows:

CO conversion for both CO and N₂ and reformate as feed:

$$\% \text{ conversion of CO } (X_{\text{CO}}) = \frac{\text{moles of CO}_{\text{in}} - \text{moles of CO}_{\text{out}}}{\text{moles of CO}_{\text{in}}} \times 100$$

H₂ selectivity for CO and N₂ as feed:

$$\% \text{ selectivity to H}_2 (S_{\text{H}_2}) = \frac{\text{moles of H}_{2\text{out}}}{(X_{\text{CO}} \times \text{moles of CO}_{\text{in}})} \times 100$$

H₂ selectivity for reformate as feed:

$$\% \text{ selectivity to H}_2 (S_{\text{H}_2}) = \frac{\text{moles of H}_{2\text{produced}}}{(X_{\text{CO}} \times \text{moles of CO}_{\text{in}})} \times 100$$

3. Results and Discussion

3.1. Preliminary Tests. Further preliminary experiments and some theoretical calculations were carried out to determine suitable conditions for which external mass transfer and internal pore mass transfer are not predominant. Considering the effect of external mass transfer, the total gas flow rate was varied between 50 and 515 mL/min under a constant residence time of 1.3 s at 873 K. As shown in Figure 1, the conversion of CO was found to be independent of the gas velocity when the gas flow rate was equal to or higher than 285 mL/min, indicating the absence of external mass transfer effects at this flow rate. This was achieved by changing the bed height from 40 to 110 mm while keeping the residence time constant.

(27) Mendis, F. M. T.; Schmal, M. *Appl. Catal.*, A **1997**, *163*, 153.

(28) Imamura, S.; Hamada, R.; Saito, Y.; Hashimoto, K.; Jindai, H. *J. Mol. Catal. A: Chem.* **1999**, *139*, 55.

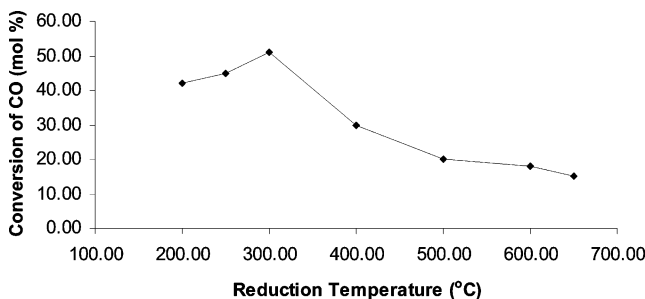


Figure 2. Effect of reduction temperature on HTS-C at a reaction temperature of 400 °C and $W/F_{A_0(\text{CO})} = 3.96$ kg (cat) h/kmol.

The calculation to determine the occurrence of any internal pore mass transfer limitation was also complemented with the theoretical work of Ibrahim and Idem,²² which was based on the derivation using the Weisz–Prater criterion as given by eq 1

$$C_{\text{wp,ipd}} = \frac{-r_{A,\text{obs}}\rho_c R_c^2}{D_{\text{eff}}C_{A_s}} \quad (1)$$

where $C_{\text{wp,ipd}}$ is the Weisz–Prater criterion for internal pore diffusion, ρ_c is the pellet density, and R_c is catalyst radius. The estimated value for $C_{\text{wp,ipd}}$ was 1.597, which is just greater than 1. According to the literature,²⁹ $C_{\text{wp,ipd}} \gg 1$ indicates a strong resistance to internal pore diffusion and can lead to a concentration gradient on the catalyst surface to its pores. On the basis of the theoretical results, the resistance to internal pore diffusion is insignificant, thus supporting our experimental results, which showed no resistance for catalyst particles less than 0.8 mm in size.

To determine whether film mass transfer resistance has any effect on the rate of reaction, the ratio of the observed rate to the rate if film resistance controls was examined. Equation 2 illustrates this criterion.

$$\frac{\text{observed rate}}{\text{rate if film resistance controls}} = \frac{-r_{A,\text{obs}}d_p}{k_c C_{A_s}} \quad (2)$$

where k_c is the mass transfer coefficient and d_p is the catalyst particle diameter. The estimated value for the ratio in eq 2 was 7.867×10^{-9} . The result indicates that the observed rate is very much lower than the limiting film mass transfer rate. Thus, the resistance to film mass transfer certainly should not influence the rate of reaction.³⁰

Similarly, internal pore heat transfer resistance was estimated using the Prater analysis given by eq 3.

$$\Delta T_{\text{max,particle}} = \frac{D_{\text{eff}}(C_{A_s} - C_{A_c})(-\Delta H_r)}{k_{\text{eff}}} \quad (3)$$

where $\Delta T_{\text{max,particle}}$ is the upper limit to temperature variation between pellet center and its surface, ΔH_r is the heat of reaction, and C_{A_s} and C_{A_c} are the concentrations at the pellet surface and center, respectively. D_{eff} is the effective mass diffusivity, and k_{eff} is the effective thermal conductivity. A value of 0.01 K was obtained for $\Delta T_{\text{max,particle}}$, which shows that the pellet more or less had a uniform temperature.

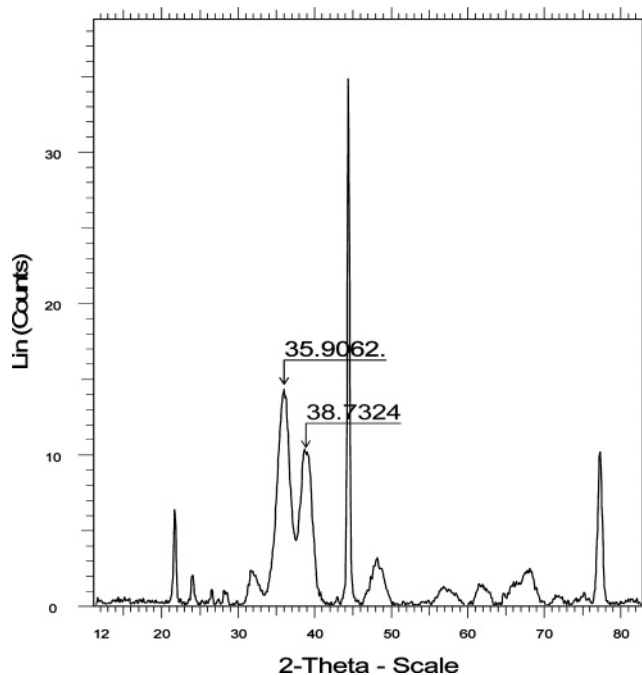


Figure 3. XRD spectra of low-temperature shift (LTS-C) catalyst.

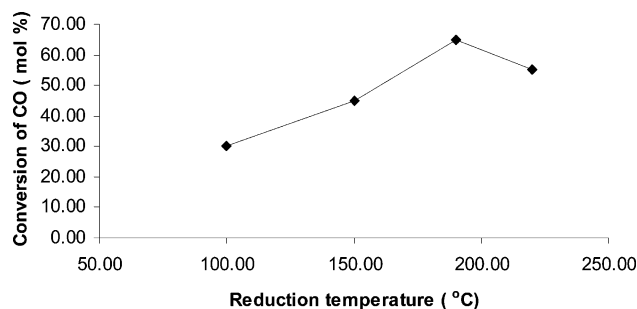


Figure 4. Effect of reduction temperature on LTS-C at a reaction temperature of 200 °C and $W/F_{A_0(\text{CO})} = 3.96$ kg (cat) h/kmol.

The heat transfer limitations across the gas film were determined using eq 4.

$$\Delta T_{\text{max,film}} = \frac{L(-r_{A,\text{obs}})(-\Delta H_r)}{h} \quad (4)$$

where $\Delta T_{\text{max,film}}$ is the upper limit to the temperature difference between the gas bulk and the pellet surface, L is the characteristic length, $r_{A,\text{obs}}$ is the observed rate of reaction, and h is heat transfer coefficient. A value of 2.98 K was obtained for $\Delta T_{\text{max,film}}$, which shows that there was a small temperature variation between the bulk temperature and the temperature of the catalyst surface. The results confirm the absence of heat transfer limitations internally, whereas an insignificant temperature gradient is observed externally. On the basis of these, isothermal operation conditions during the reaction were assumed.³⁰

3.2. Effect of Reduction Temperature. For activation, both the HTS-C and LTS-C need to be reduced prior to use. The literature suggests the reduction temperature range of 250–400 °C for Fe–Cr types of HTS-C catalysts. A higher temperature results in sintering of the catalyst and activity loss. It has been realized that the activity and thermostability of the iron catalyst is connected with the crystal structure of iron oxide species such as hexagonal $\alpha\text{-Fe}_2\text{O}_3$ and cubic $\gamma\text{-Fe}_2\text{O}_3$. Because of the low activation energy involved with $\gamma\text{-Fe}_2\text{O}_3$ species, it was found to be more active for the WGS compared to $\alpha\text{-Fe}_2\text{O}_3$. However,

(29) Fogler, H. S. *Elements of Chemical Reaction Engineering*, 3rd ed.; Prentice Hall: Englewood, Cliffs, NJ, 1999.

(30) Levenspiel, O. *Chemical Reaction Engineering*, 3rd ed.; Wiley: New York, 1999.

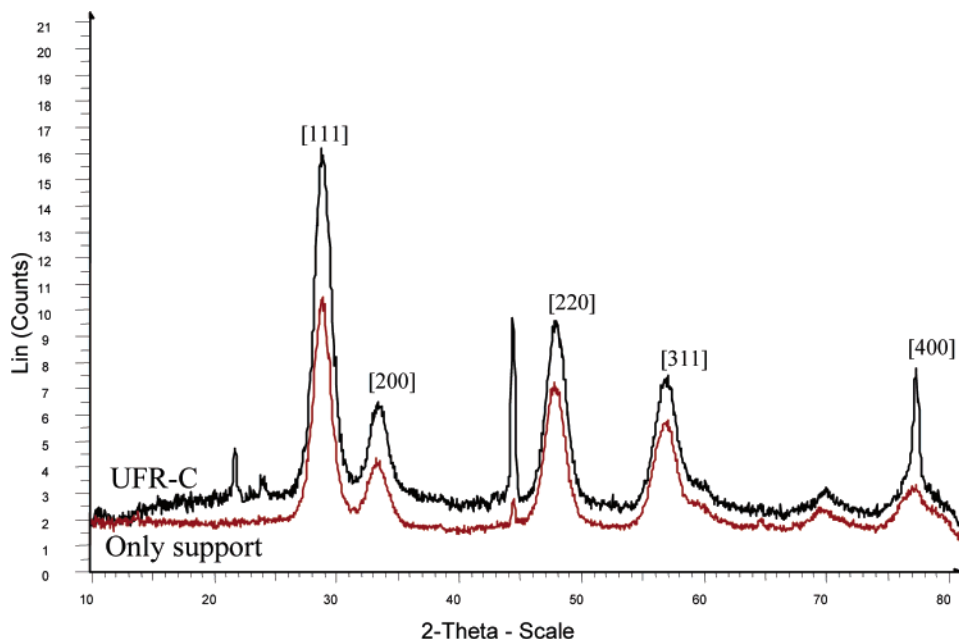


Figure 5. XRD pattern for the UFR-C catalyst and the support.

the crystal defect generally found in the imperfect cubic spinel structure allows Cr to be incorporated into the vacant sites in the γ - Fe_2O_3 , resulting in less sintering of the active phase in the catalysts consisting of γ - Fe_2O_3 than in those containing α - Fe_2O_3 under identical operating conditions. It is also observed that the transition of the γ - Fe_2O_3 phase into the more stable α - Fe_2O_3 phase is possible at a higher temperature.³¹ The HTS-C catalyst loses its activity when the reduction temperature is increased from 200 to 650 °C, as seen in Figure 2. This could be attributed primarily to the phase transition from γ - Fe_2O_3 to α - Fe_2O_3 facilitated at a high temperature.³² We did not observe any XRD fingerprint on the HTS-C sample. Thus, it is difficult to conclude that, at a temperature of about 300 °C, the concentration of γ - Fe_2O_3 is at maximum.

On the other hand, Cu-based catalysts (LTS-C), considered better than the Pt- and Au-based catalysts in terms of H_2 selectivity and thermal stability while operating at significantly lower reaction temperatures, are also very sensitive to the reduction temperature. Generally, the temperature range of 180–250 °C is suggested in the literature, attributed largely to the reduction of larger CuO particles.¹¹ In some cases, reduction temperatures even lower than 200 °C have been reported, if the CuO particles sizes were very small. This can be seen in the XRD fingerprints of the LTS-C sample given in Figure 3 where the intense reflection of CuO (JCPDS 45-0937) at 2θ values of 35.9° and 38.7° is observed. However, these bulk CuO particles must coexist with the dispersed copper oxide to trigger the WGS activity. It can be seen in Figure 4 that the reduction at ca. 190 °C results in maximum conversion under our experimental conditions, which could be partly due to well-dispersed copper oxide even though the latter is mainly present as relatively large CuO particles in the commercial LTS-C catalyst. As reported¹¹ in some cases, the active ingredient of the catalyst is not the metallic copper but the copper ions in the dispersed state. At higher temperatures, probably the formation of spinel structures leads to low activity.

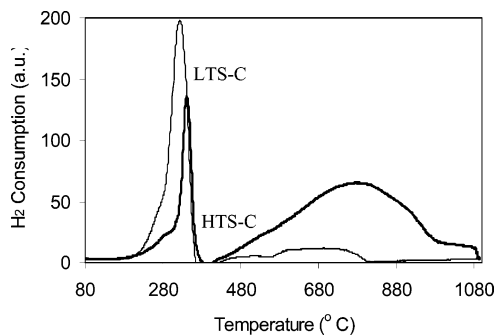


Figure 6. TPR profiles of both HTS-C and LTS-C catalysts.

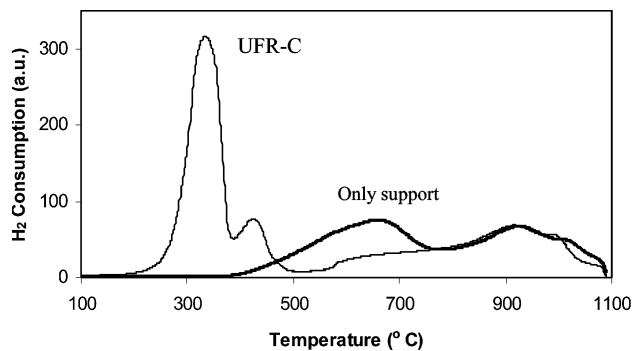


Figure 7. TPR profiles of both the UFR-C catalyst and the support.

The UFR-C catalyst developed in house is also characterized using XRD for phase purity determination. The XRD patterns after calcinations of UFR-C along with the support (Figure 5) indicate the presence of a true mixed-oxide phase with the cubic structure. There is also no evidence of any crystallite formation of either nickel or copper on the support, indicating a monolayer and high dispersion of the base metals on to the support. This makes the catalyst UFR-C distinctly different from the HTS-C and LTS-C catalysts, although all are copper-promoted to certain extents.

Further, the reducibility of the catalysts was studied using TPR to determine the textural changes of the material and

(31) Kundu, M. L.; Sengupta, A. C.; Maiti, G. C. *J. Catal.* **1988**, *112*, 375.

(32) Li, S.; Li, A.; Krishnamoorthy, S.; Iglesia, E. *Catal. Lett.* **2001**, *77* (4), 197.

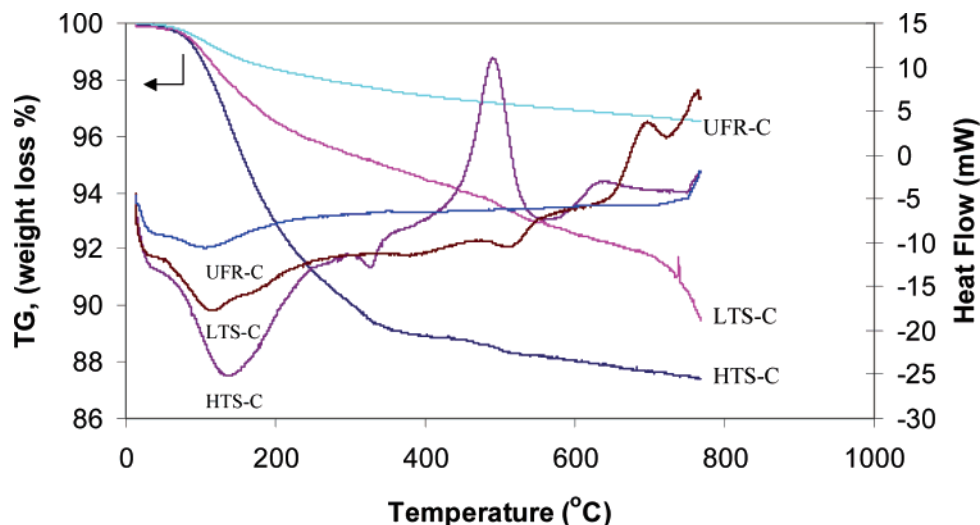


Figure 8. TG/DSC profiles of UFR-C, HTS-C, and LTS-C catalysts.

oxygen diffusion in the lattice structure. The TPR profile of the HTS-C catalyst as presented in Figure 6 revealed two distinct peaks. The one small shoulder at 280 °C was attributed to the reduction of CuO, while the main peak at about 370 °C was generally associated with the reduction of Fe₂O₃. It means the reduction temperature between 300 and 350 °C would be better if the catalyst is to be used at high temperatures. The TPR profile (Figure 6) of the low-temperature catalyst, LTS-C, also revealed a very similar observation. The one small shoulder at 200 °C was ascribable to a reduction of Cu²⁺ to Cu, and a broad peak between 250 and 440 °C was observed, indicating a superimposition of several peaks which can represent different kinds of Cu²⁺ in the commercial LTS-C catalyst. Cu²⁺ in the ZnO lattice, in amorphous Cu oxide phases, in crystalline CuO, and in the Al₂O₃ phases could be the possible sources of the broad superimposition of the peaks. For comparison, the TPR profile of the UFR-C catalyst and support is presented in Figure 7. A broad single peak between 400 and 650 °C can be seen, which is generally identified with the ceria–zirconia mixed-oxide system when the insertion of ZrO₂ into the CeO₂ lattice leads to the formation of a solid solution.²⁶ Surface and bulk reductions (as present in CeO₂) are indistinguishable by the TPR technique in the ceria–zirconia solid solution because of comparable reduction energy.^{32,33} On the other hand, the bimetallic UFR-C catalyst shows increased hydrogen consumption in the low-temperature region. The two very distinguishable peaks centered at 350 and 420 °C can be assigned to the highly dispersed CuO and NiO species in close contact with the support, respectively, clearly indicating the promoting effect of the reduction of the surface oxygen species. No evidence for peaks attributable to support reduction has been detected in the range of 500–750 °C, that is, at temperatures where the reduction of the support was observed, because of thermodynamic constraints, as recently reported.³⁴ On the basis of these observations, only one reduction temperature (650 °C) was used for the water–gas shift reaction using UFR-C as the catalyst.

3.3. Effect of Reaction Temperature. Both HTS-C and LTS-C catalysts are temperature-sensitive. This can be seen in Figure 8 where the TG/DSC profiles of the HTS-C, LTS-C, and UFR-C catalysts are presented. For the HTS-C catalyst, two stages of weight loss can be observed in the TGA curves;

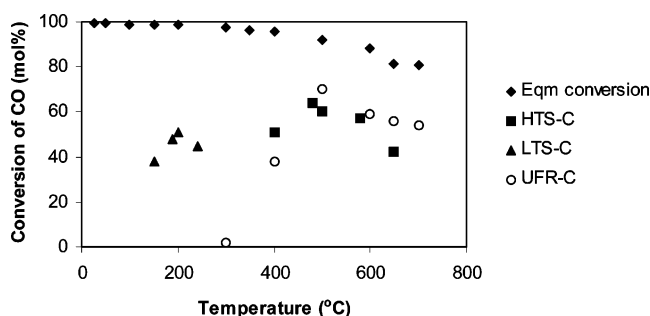


Figure 9. Effect of reaction temperature on HTS-C and LTS-C catalysts at W/F_{A0(CO)} = 3.96 kg (cat) h/kmol.

the first stage of weight loss of about 10% is observed between 0 and 190 °C, and the second stage of weight loss of about 1–2% is observed above 320 °C. This corresponds to the two endothermic peaks on the DSC profiles, demonstrating that the decomposition of water and carbonates proceeded in two steps. Two exotherms are also observed in Figure 8: a large one occurring between 450 and 500 °C and a small one occurring between 625 and 650 °C which could be related either with the agglomeration of γ -Fe₂O₃ and α -Fe₂O₃ phases present in the catalyst or the formation of some inactive spinel structures. This means a temperature higher than 500 °C would be detrimental for the HTS-C catalysts. Similarly, the TG/DSC profile of LTS-C results in three endothermic and one exothermic peak (Figure 8). Three stages of weight loss can be observed in the TGA curves; the first stage of weight loss of about 4% is observed between 0 and 120 °C, and the second and third stages of weight loss of about 1–2% are observed above 350 and 500 °C, respectively. This also corresponds to the first endothermic peak at ca. 109 °C, indicating the solid–solid first phase transition as seen on the DSC profiles. The only exothermic peak at about 680 °C again indicates the formation of catalytically inactive spinel structure. On the basis of this result, it can be said that the desirable temperature for the LTS catalysts should be lower than 200 °C. The catalyst UFR-C did not show any appreciable weight loss or phase transition as indicated from the TG/DSC profile.

The WGS activities at different temperatures for all three catalysts are further presented along with the equilibrium conversion at different temperatures in Figure 9. The reduction temperatures for LTS-C and HTS-C catalysts were 190 and 300 °C, respectively, while for UFR-C, the reduction temperature was 650 °C. It can be seen that HTS-C gives the maximum

(33) Vidal, H.; Kaspar, J.; Pijolat, M.; Colon, G.; Bernal, S.; Cordon, A.; Perrichon, V.; Fally, F. *Appl. Catal., B* **2000**, *27*, 49.

(34) Di Monte, R.; Kaspar, J. *J. Mater. Chem.* **2005**, *15*, 633.

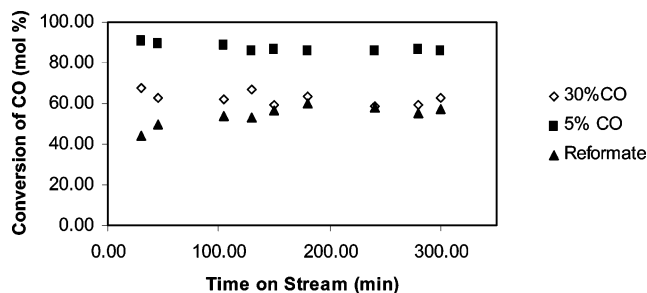


Figure 10. Effect of CO on HTS-C catalyst at a temperature of 500 °C at $W/F_{A0(CO)}$ values of 3.96, 12.49, and 5.02 kg (cat) h/kmol for 30% CO, 5% CO, and reformate, respectively.

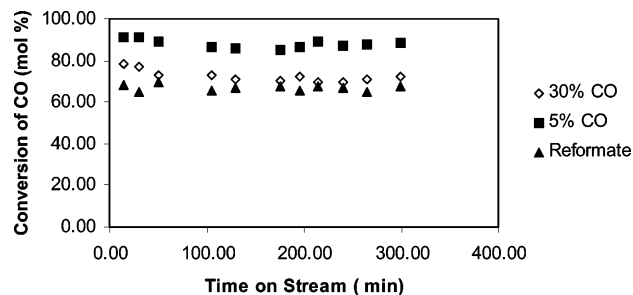


Figure 11. Effect of CO on the UFR-C catalyst at a temperature of 500 °C at a $W/F_{A0(CO)}$ of 3.96 kg (cat) h/kmol for 30% CO, 5% CO, and reformate.

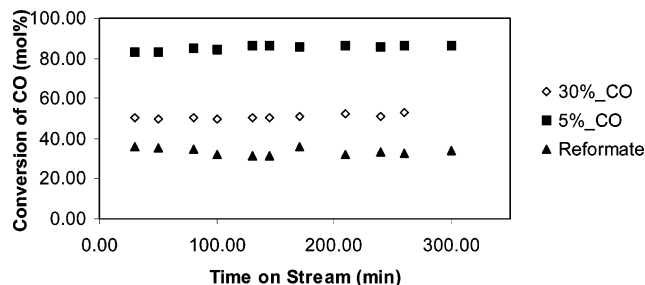


Figure 12. Effect of CO on the LTS-C catalyst at a temperature of 200 °C at $W/F_{A0(CO)}$ values of 3.96, 5.02, and 24.98 kg (cat) h/kmol for 30% CO, 5% CO, and reformate, respectively.

conversion at 480 °C, and LTS-C gives a maximum at about 190 °C. These results are consistent with the TG/DSC data as well. Overall, the WGS activity for UFR-C at high temperatures was relatively better than that of the commercial HTS-C catalyst. The activity was found to improve when smaller particles of the catalyst were used.

3.4. Effect of CO Concentration. The effect of CO concentration on the catalytic activity of all three catalysts in the WGS reaction was also studied, and this is illustrated in Figures 10 and 11 for HTS-C and UFR-C at 500 °C, respectively, while Figure 12 represents similar data for LTS-C at 200 °C. In these experiments, the concentration of CO (inlet mole fraction of CO) was varied from 0.026 to 0.168, keeping the water concentration fixed at 0.455 and the rest being nitrogen with a fixed catalyst weight of 0.5 g. This was achieved by using three different types of feed, namely,¹ 5% CO in nitrogen,² 30% CO in nitrogen, and³ 24% CO in reformate. As shown in Figure 10, there is a significant effect of CO concentration on the activity of the WGS reaction using the HTS-C catalyst. At 5% CO in the feed, CO conversion reaches a maximum of 95%. The conversion is drastically reduced when the CO concentration is increased. However, the presence of reformate in CO does not affect the conversion at 500 °C. On the other hand, the UFR-C catalyst under similar reaction conditions gave a far

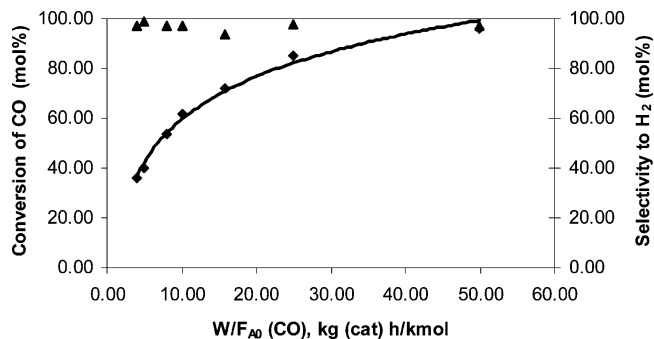


Figure 13. Conversion of CO and H₂ selectivity as a function of $W/F_{A0(CO)}$ for LTS-C at reduction temperature = 200 °C, reaction temperature = 200 °C, and WHSV = 2320 h⁻¹ and feed = 30% CO and balance N₂.

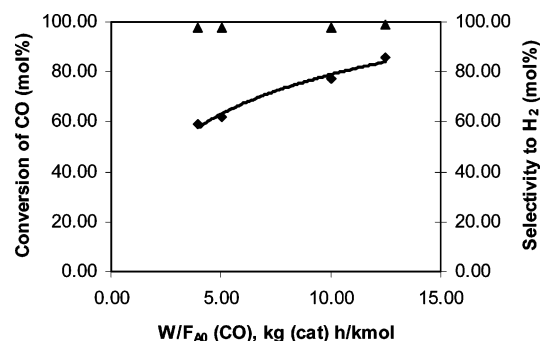


Figure 14. Conversion of CO and H₂ selectivity as a function $W/F_{A0(CO)}$ for HTS-C at reduction temperature = 300 °C, reaction temperature = 500 °C, and WHSV = 3300–3800 h⁻¹ and feed = 30% CO and balance N₂.

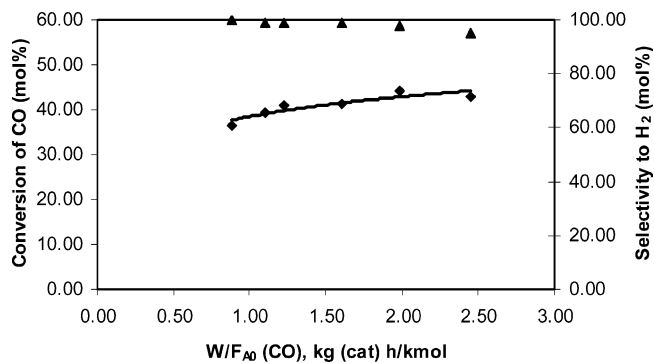


Figure 15. Conversion of CO and H₂ selectivity as a function $W/F_{A0(CO)}$ for UFR-C at reduction temperature = 650 °C, reaction temperature = 500 °C, and WHSV = 3500–9600 h⁻¹ and feed = 30% CO and balance N₂.

better performance at all CO concentrations (Figure 11) at the same temperature, indicating a better and robust catalyst in the form of UFR-C. A similar effect was also observed on LTS-C catalysts at 200 °C (Figure 12) under similar conditions, although the conversion of CO was lower compared to those for both UFR-C and HTS-C. Similar results were also obtained on the effect of CO concentration on other different types of catalysts available in the literature.^{35,36}

3.5. Effect of $W/F_{A0(CO)}$. Further evaluations of the catalysts were carried out to study the effect of $W/F_{A0(CO)}$ in the range of 3.96–49.96 kg (cat) h/kmol on CO conversion with a corresponding gas hourly space velocity of 2320 h⁻¹ for LTS-C

(35) Rethwisch, D. G.; Dumesic, J. A. *Appl. Catal.*, A **1986**, 21, 97.

(36) Saito, M.; Murata, K. *Catal. Surv. Asia* **2004**, 8 (4), 285.

Table 2. The Best Reaction Condition^a for the Highest Activity for the Different Catalysts^b

catalyst	X_CO (mol %)		S_H ₂ (mol %)		Y_H ₂ (mol %)		reduction temp (K)	reaction temp (K)
	gas 1	gas 2	gas 1	gas 2	gas 1	gas 2		
LTS-C	63	70	100	100	63	70	463	473
HTS-C	64	67	98	100	63	67	573	753
UFR-C	5	3.5	100	100	5	3.5	923	573
UFR-C	62	58	97	92	60	53	923	673
UFR-C	66	88	97	94	64	83	923	773
UFR-C	69	85	99	93	68	79	923	873
UFR-C	72	77	100	91	72	70	923	923
UFR-C	71	75	100	91	71	68	923	973

^a Using the powder catalyst (particle size = 150 μm). ^b Gas 1 = reformat mixture (24 wt % CO, 1.5 wt % CO₂, 2.5 wt % H₂, 2 wt % CH₄, and balance N₂). Gas 2 = 30 wt % CO and balance N₂.

(at the reaction temperature of 200 °C) and between 3300 and 3800 h⁻¹ for HTS (at the reaction temperature of 500 °C) catalysts. For LTS-C, the results are presented in Figure 13, which shows that the conversion of CO increased from 36 mol % for a W/F_{A0(CO)} ratio of 3.96 h to 96 mol % for a W/F_{A0(CO)} ratio of 49.96 h. Similar results were also obtained for HTS-C catalysts, as presented in Figure 14, where CO conversion only marginally increased with respect to increasing contact time. It means that the CO conversion increases with increasing contact time of CO in the reactor for both the catalysts, as expected. H₂ selectivity on the other hand was almost constant at different contact times. Similar data for the UFR-C catalyst at 500 °C and having a weight-hourly space velocity (WHSV) in the range of 3500–9600 h⁻¹ give a slightly different performance at a very short contact time (Figure 15) compared to commercial catalysts.

3.6. Overall Performance. On the basis of the results, the overall performance of the catalysts can be summarized for both commercial grade HTS-C and LTS-C as well as for UFR-C catalysts for WGS reaction under the established reaction conditions. The results are compared in Table 2 where the

activities of the catalyst developed in our laboratory are presented along with those of the commercial catalysts at different temperatures. It can be seen that, under the reformat conditions, the activities of the UFR-C catalyst were better compared to those of HTS-C at the same temperature and even improved at relatively higher temperatures, while in the case of pure CO as a feed, UFR-C gave a much better performance compared to the two commercial catalysts at all temperatures. As all three catalysts are Cu-promoted, the better dispersion and highest surface area of the Cu particles in the case of UFR-C indicate a smaller Cu particle, which probably shows that there is a proportional relation between catalytic activity and copper surface area. Further, the developed UFR-C catalyst was found to be very stable, withstanding reaction conditions above 700 °C with no detectable deactivation over many hours of operation. On the basis of the kinetics experiments on UFR-C under the reaction conditions established, no evidence of either heat and mass transfer or pore diffusion limitations were observed.

4. Conclusions

We have demonstrated that the water–gas shift activities of the copper-promoted commercial catalysts are not suitable for performance at high temperatures. Under the reformat conditions, UFR-C was found to be more stable with no apparent activity loss compared to both HTS-C and LTS-C catalysts. The superior catalytic performance of UFR-C is attributed to the existence on the catalytic surface of higher amounts of easily reducible well-dispersed copper and nickel oxide species strongly interacting with the support material. The kinetics and derivation of the rate equation as well kinetic models along with other characterization data on the UFR-C catalyst such as X-ray photoelectron spectroscopy, X-ray absorption spectroscopy, and scanning transmission electron microscopy are under progress and will be reported separately.

EF060389X